Soils and Foundations 2012;52(4):698–711

The Japanese Geotechnical Society

Soils and Foundations

www.sciencedirect.com
journal homepage: www.elsevier.com/locate/sandf

Strength reduction of cohesionless soil due to internal erosion induced by one-dimensional upward seepage flow

Lin Ke, Akihiro Takahashi*

Tokyo Institute of Technology, Japan

Received 20 October 2011; received in revised form 2 May 2012; accepted 20 June 2012
Available online 30 August 2012

Abstract

Suffusion, one of the modes of internal erosion, has been widely detected in both natural deposits and filled structures. It is the phenomenon that the fine particles in soil gradually migrate through the voids between the coarse particles, leaving behind the soil skeleton. In this paper, the main focus is on the changes in soil strength due to internal erosion. A series of one-dimensional upward seepage tests at a constant water head is performed to cause internal erosion in a soil sample by controlling the three variable parameters, namely (a) the fine content, (b) the relative density of the soil, and (c) the maximum imposed hydraulic gradient on the specimen. The mechanical consequences of the internal erosion are examined by cone penetration tests. The internal erosion indicated by the loss of fine particles causes changes in the void ratio and a significant increase in hydraulic conductivity, resulting in a decrease in the soil strength from its initial value.

Keywords: Internal erosion; Suffusion; Upward seepage test; Hydraulic conductivity change; Strength reduction

1. Introduction

Seepage-induced erosion, resulting from soil particle migration, is widely observed in both natural soil deposits and artificially engineered fill structures. The most significant influence of seepage erosion is on the earth dams, the failure of which could have catastrophic consequences. Gap-graded cohesionless soil is especially vulnerable to internal erosion due to its deficiency in particle size. This kind of material has played a significant role in the potential for seepage-induced internal erosion.

In the literature, the term "internal erosion" usually refers to the detachment of soil particles from the main soil structure due to the mechanical or the chemical action of a fluid flow. The "internal erosion" customarily includes "suffusion" and "piping" phenomenon. In suffusion, the fine particles are eroded through the voids between the larger particles by the seepage flow, leaving behind the coarse skeleton, while the progressive erosion and transportation of soil particles along a flow path indicate the phenomenon of piping. Suffusion and piping may lead to obvious changes in porosity, a significant increase in hydraulic conductivity and the potential for a reduction in soil strength. Suffusion and piping are always coupled phenomenon. The common term "internal erosion" is used here to describe the target phenomenon that small particles are washed out through the voids between the coarse particles by the seepage flow, leaving behind the soil skeleton.

The hydrological mechanism of internal erosion has been widely investigated. Changes in the hydraulic gradient (the critical hydraulic gradient) and in hydraulic conductivity, as well as a loss in fine particles, were the primary concerns. The initial systematical experimental investigations consisted of base soil and filter compatibility studies (Terzaghi and Peck,

*Corresponding author.
E-mail address: takihiro@cv.titech.ac.jp (A. Takahashi).
Peer review under responsibility of The Japanese Geotechnical Society.

Production and hosting by Elsevier

0038-0806
http://dx.doi.org/10.1016/j.sandf.2012.07.010

1948; US Army Corps of Engineer, 1953; Istomina, 1957; Kenney and Lau, 1985, 1986; among others). By recognizing the effective particle size ratio between the base soil and the filter, many empirical methods, namely geometrical criteria, were proposed to prevent soil erosion and to allow for water seepage. The phenomenon that the base soil or the filter, which satisfies the geometrical criteria, could fail because of the internal erosion of fine particles, led to soil internal instability studies (Skempton and Brogan, 1994; Tomlinson and Vaid, 2000; Moffat and Fannin, 2006; among others). In those experimental investigations, not only the geometric characteristics of the soil, but also the influence of other factors on the internal erosion, have been considered, such as flow velocity, flow direction and the hydraulic gradient. The tested soils were "poor-graded" soils, which means gap-graded or widely graded coarse soils. The main apparatus usually contained a permeameter together with measurement of the pore water pressure to characterize hydromechanical spatial variations and vertical load to obtain the effective stress distribution along the specimen. The particle erosion rate and the possible chemical reactions, if any, were also measured.

Internal erosion occurs if the following criteria are satisfied (Wan, 2006): (a) the size of the fine particles is smaller than the size of the voids between the coarse particles, which form the skeleton of the soil, and the amount of fine particles is less than enough to fill the voids between the coarse particles (geometrical criteria) and (b) the hydraulic gradient is large enough to move the fine soil particles through the voids between the coarse particles (hydraulic criterion).

The hydro-mechanical properties of soil, such as the internal erosion onset hydraulic gradient, may be closely related with the fine content. Experimental research has also indicated that changes in the fine content may cause either a decrease or an increase in soil strength. The soil behavior seems to be dependent on the range in fine contents, which may possibly explain the changes in soil strength after internal erosion. Due to the difficulties of describing the fine content-dependent soil behavior by the "void ratio" concept alone, Thevanayagam and Mohan (2000) proposed "intergranular void ratio" by assuming that the volume of fines is a part of the voids between the coarser particles. If the difference in specific gravity between the coarser and the finer particles is disregarded, the "intergranular void ratio, e_s'', can be obtained from the void ratio and the fine content. On the basis of a demarcation line corresponding to $e_s=e_{max,HS}$ (maximum void ratio of the coarse particles), the soil behavior, which depends on the combination of the void ratio and the fine content, is divided into three cases (cf. Fig. 4). Case 1 has a relatively smaller void ratio and a smaller fine content. In this case, the intergranular void ratio of the soil specimen is smaller than the maximum void ratio of the coarse particles. Most of the fines are locked in the intergranular voids. The soil behavior largely depends on the coarse materials. Case 3 has a relatively larger void ratio. The intergranular void ratio is larger than the maximum void ratio of the coarse particles. In this case, the coarse particles are separated by the fines, leading to a relatively unstable soil structure. The shear strength of the soil could be significantly influenced by the shear resistance along the fines. Case 2 has an intermediate void ratio. The intergranular void ratio is approximately equal to the maximum void ratio of the coarse particles. The anticipated soil behavior would depend on whether or not the fines are locked in the intergranular voids or work as separators between the coarse particles. Vallejo (2001) explained the changes in strength of binary mixtures by porosity and the mixture structure. The soil structure is characterized by coarse particles when the coarse particle concentration is greater than 70%, while the fine particles dominate if the coarse particle concentration is less than 40%. In between them, both coarse and fine particles partially characterize the soil structures. The shear strength of a binary mixture is directly influenced by the frictional strength between the particles which hold the structures. To shed light on the strength–deformation properties of binary mixtures, Omine and Ochiai (1992) and Omine et al. (1996) proposed a two-phase mixture model. In this model, a new parameter, corresponding to the volume content of the fines, is introduced to evaluate the stress distribution in mixtures. By assuming that the strain energy increments of fines and the matrix per unit volume are equal, the incremental stress–strain relationship of the mixtures could be derived based on the new parameter. The validity of this model is confirmed by the results of unconfined compression tests on mixtures of expanded polystyrol and kaolin clay. It is found that the unconfined compressive strength of the mixtures decreases with an increase in the volume content of the expended polystyrol pieces.

The primary purpose of this study is to evaluate the reduction in soil strength after internal erosion. The hydraulic conditions which trigger internal erosion, with reference to the influence of the fine particle content, the relative density and the imposed hydraulic gradient, are obtained through a series of upward seepage tests. A multi-stage test procedure is conducted to assess the conditions necessary for triggering internal erosion. The changes in strength of the soil subjected to internal erosion are evaluated by a cone tip resistance profile from cone penetration tests (CPTs).

2. Upward seepage test

2.1. Tested materials

According to previous studies, soils with a "fine fraction" and a "coarse fraction" are vulnerable to internal erosion. The binary mixtures in this study consist of two Silica sands (Silica nos. 3 and 8) having different dominant particle sizes. With a larger particle size, the Silica no. 3 works as the coarse particles, while the fine Silica no. 8 is the erodible fine particles. The siliceous sand used here is mainly composed of quartz, categorized as an angular to sub-angular material. Particle size distribution, specific gravity, maximum and minimum void ratios and hydraulic conductivity are summarized in Fig. 1 and Tables 1 and 2.

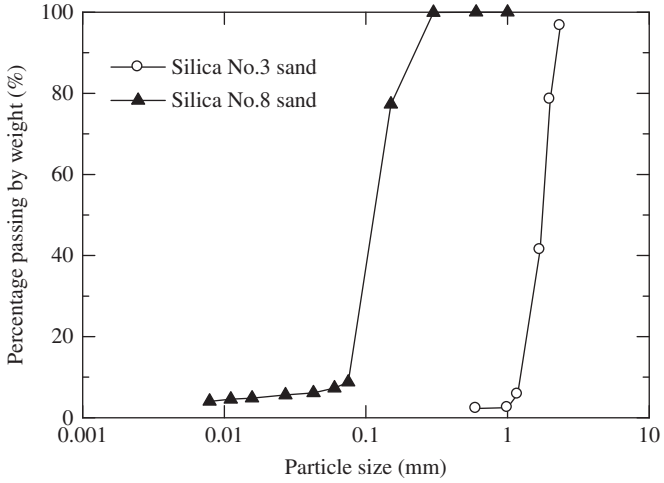

Fig. 1. Particle size distribution curves for Silica nos. 3 and 8.

Table 1
Sand particle size distribution parameters.

Property	Silica no. 3	Silica no. 8
Median particle size D_{50} (mm)	1.72	0.16
Effective particle size D_{10} (mm)	1.37	0.087
Uniformity coefficient C_u	1.29	2.09
Curvature coefficient C_c	0.99	2.34

2.2. Test specimens

The primary target of the seepage tests is to create internally eroded saturated soil specimens. To this end, the initial conditions of those test specimens have to meet the criteria of the above-mentioned onset of internal erosion. The geometrical criteria can be satisfied if the phase relationship between the coarse particles and the fine particles, shown in Fig. 2, are considered.

The mass balance of the soil can be expressed as

$$f_s + f_f = 1 \tag{1}$$

where f_s is the mass ratio of the coarse particles, equaling $W_s/(W_s+W_f)$, and f_f is the mass ratio of the fine particles, equaling $W_f/(W_s+W_f)$.

Assuming all the fine particles are erodible, the coarse particle void ratio is

$$e_s = (V_w + V_f)/V_s \tag{2}$$

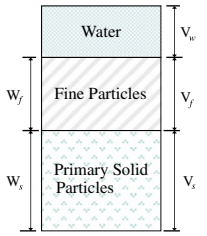

Symbols mean:
V_s: Volume of coarse particles forming the primary fabric of soil;
V_f: Volume of erodible fine particles filling in the voids between coarse particles;
V_w: Volume of water;
W_s: Weight of coarse particles;
W_f: Weight of erodible fine particles.

Fig. 2. Schematic phase diagram of saturated binary soil.

and the fine particle void ratio is

$$e_f = V_w/V_f \tag{3}$$

From Eqs. (1)–(3), and assuming that the specific gravities of the coarse and the fine particles are the same, the following equation is obtained:

$$f_f = e_s/(1+e_s+e_f) \tag{4}$$

Eq. (4) indicates that the possible maximum value for f_f is reached under ideal conditions, namely the coarse particles in the binary mixture specimen are loosely packed, while the fine particles are densely packed inside the voids between the coarse particles. Since the maximum void ratio of the no. 3 sand is 1.009 (the primary fabric formed by Silica no. 3 is loosely packed) and the minimum void ratio of Silica no. 8 is 0.703 (the fine particles, Silica no. 8, are densely packed), the possible maximum mass ratio of the erodible fines is 37%. A series of four binary mixtures is determined as the test soils based on the above calculation. The fine contents of the four mixtures are 25%, 20%, 16.7% and 14.3%, respectively, which are less than the calculated possible maximum value. The particle size distributions, the specific gravity, and the maximum and minimum void ratios of the four tested soils are shown in Fig. 3 and Table 3.

To ensure that internal erosion will occur during the seepage tests, the vulnerability of the four mixture soils to internal erosion is assessed by five currently available methods proposed by US Army Corps of Engineers (1953), Istomina (1957), Kenney and Lau (1985, 1986), Burenkova (1993) and Mao (2005). The results are summarized in Table 4. The four

Table 2
Specific gravity, maximum void ratio, minimum void ratio and hydraulic conductivity of Silica sand.

Properties	Specific gravity	Maximum void ratio (e_{max})	Minimum void ratio (e_{min})	Hydraulic conductivity (m/s)		
				30%[a]	60%[a]	80%[a]
Silica no. 3	2.63	1.009	0.697	6.6×10^{-3}	5.6×10^{-3}	4.9×10^{-3}
Silica no. 8	2.63	1.333	0.703	3.4×10^{-5}	2.6×10^{-5}	2.1×10^{-5}

[a]Relative density.

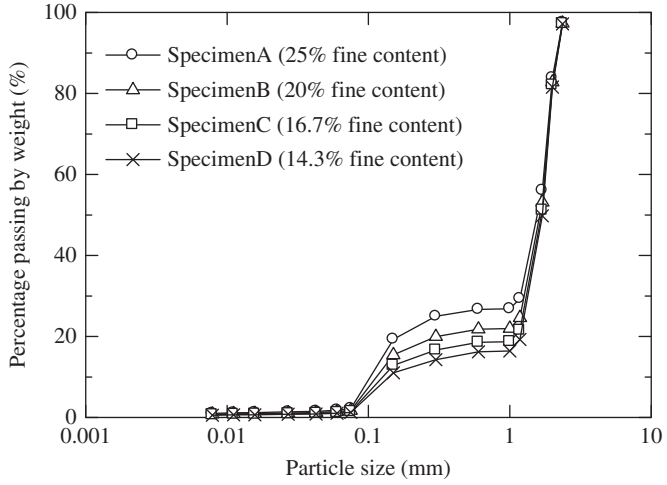

Fig. 3. Particle size distributions of four soils.

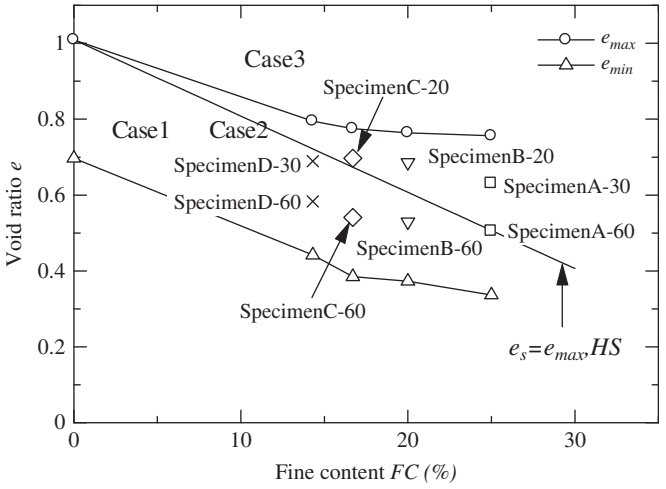

Fig. 4. Intergranular matrix phase diagram.

Table 3
Sand parameters of the four specimens.

Properties	Specimen A	Specimen B	Specimen C	Specimen D
Specific gravity	2.63	2.63	2.63	2.63
Maximum void ratio	0.756	0.764	0.775	0.795
Minimum void ratio	0.367	0.373	0.385	0.402
Void ratio range[a]	0.389	0.391	0.39	0.393

[a]Difference in void ratio between loosest and densest sand states.

Table 4
Assessment of specimen vulnerability to internal erosion by current methods.

Specimen	Methods used to assess internal stability				
	US Army (1953)	Istomina (1957)	Kenney and Lau (1986)	Burenkova (1993)	Mao (2005)
A	S	S	U	U	U
B	S	S	U	U	U
C	S	S	U	U	U
D	U	U	U	U	U

Note: "U" means unstable; "S" means stable.

soils are potentially unstable and vulnerable to internal erosion if seepage takes place.

2.3. Selection of relative densities of specimens

A plot of void ratios against fine contents is shown in Fig. 4. The demarcation line, located between the maximum and the minimum void ratio lines, is determined by $e_s=e_{max,HS}$ (Thevanayagam and Mohan, 2000), where intergranular void ratio e_s is defined as

$$e_s=\frac{e+FC}{1-\mathrm{FC}} \tag{5}$$

Table 5
Seepage test specimens.

Specimen no.	Fine particle content (%)	Relative density (%)	Void ratio
A-30	25	30	0.63
A-60	25	60	0.51
B-20	20	20	0.69
B-60	20	60	0.53
C-20	16.7	20	0.70
C-60	16.7	60	0.54
D-30	14.3	30	0.69
D-60	14.3	60	0.58

e is the soil void ratio and FC is the fine content. The soil behavior around this line may be influenced by both coarse particles and fines. If those fines which actively play a role in transferring loads are eroded, the soil strength may be changed accordingly. In this series of tests, the relative densities of the specimens are expected to cover this demarcation line. Two different relative densities are finally selected for each soil specimen, as shown in Fig. 4 and Table 5.

2.4. Test apparatus

Constant head seepage tests with upward water flow are performed to cause internal erosion. A schematic diagram of the seepage test apparatus is shown in Fig. 5. The cylindrical seepage cell is 100 mm in internal diameter and 300 mm in height. The transparent seepage cell allows for the observation of the internal erosion from the side. The upper end of the seepage cell is left open so that the erosion process can be observed from the top. An overflow pipe is fitted at the top portion of the seepage cell to manually measure the flow rate by a cylinder. Two 10-mm-thick plastic rings with waterproof tape are set separately on the top and the bottom of the specimen to prevent the formation of large seepage channels between the soil and

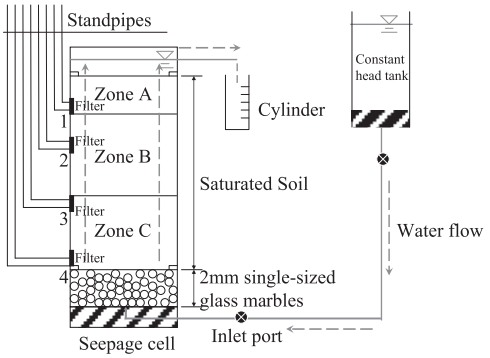

Fig. 5. Schematic diagram of seepage test assembly.

the side wall. The layer consisting of 2-mm single-sized glass balls underneath the 170-mm-thick specimen serves to break up the incoming flow to ensure a uniform water flow on the specimen. Nonwoven textile is placed at the bottom of the specimen to prevent downward fine particle loss. The variation in water head within the specimen is measured by four stand pipes at four different depths, 20 mm, 50 mm, 105 mm and 165 mm. The inlet is connected to a constant water head tank, which can be raised or lowered to control the hydraulic gradient across the specimen, while the outlet is open to the atmosphere.

2.5. Specimen preparation

To prevent the segregation of the two different sized particles, the moist tamping method is employed (Ladd, 1978; Frost and Park, 2003). This method achieves uniform specimens by the concept of "undercompaction": each layer is compacted to a lower density than the desired value by a predetermined amount due to the fact that the compaction of succeeding sand layers would also densify the layers below. It has been proven reliable by other scholars (Bradshaw and Baxter, 2007; Yang et al., 2008). The sample preparation procedures are as follows: determine the oven-dried weights of both Silica nos. 3 and 8 for tests according to the prescribed fine content and relative density. Adjust the water content to an appropriate value. Usually, for the larger fine content specimen, a greater water content is preferred (e.g., the initial water content of Specimen A is 8%, while that of Specimen D is 5%). Thoroughly mix the soils with water to ensure that the fine particles are distributed as uniformly as possible. This procedure is usually done at least 16 h before use. The specimen is prepared layer by layer. Weigh the amount of material required for each layer, and place it into the cell with a scoop. A tamping rod is used to compact the soil to the required height determined by "undercompaction". Upon completion, weigh the specimen to check the relative density again and record it. This process usually takes two hours. Saturation of the specimen is performed in a vacuum tank. De-aired water is purged into the specimen from the bottom inlet at a slow rate. This process takes approximately 5–6 h to ensure saturation quality.

Test procedure

A series of tests is conducted following the multi-stage procedure. Each test usually takes 5–6 h depending on the imposed hydraulic gradient. The detailed test procedure is as follows:

(1) Before the test, check the position of the water level of the four standpipes to make sure the initial water head of all four is the same. Adjust the level of the constant water head tank to ensure that its water table is the same as that of the seepage cell.
(2) The initially imposed hydraulic gradient is usually in the range of 0.05–0.1. Increase the hydraulic gradient at approximately the same increments. When the hydraulic gradient reaches around the value required to cause initial internal erosion, the increment could be relatively smaller.
(3) For each step, allow 30 min to ensure the completion of the internal erosion, i.e., the discharge rate is stable and the effluent color becomes clear. Record the water head distribution from the stand pipes. Estimate the discharge rate by measuring the volume of discharge effluent per minute three times. Record the water temperature. Carefully observe the phenomena occurring during the test, such as the flow turbidity, the jumping, the piping or the transportation of the fine particles, and record them with a camera.
(4) Repeat (2) and (3) until the soil becomes unstable, e.g., the specimen shows "boiling", or until the largest achievable hydraulic gradient is imposed if instability does not occur.

3. Upward seepage test results and discussion

3.1. Definitions

Two types of critical hydraulic gradients are presented.

A critical hydraulic gradient for soil stability i_c was proposed by Terzaghi to determine a zero effective stress condition. It is related to the void ratio and the specific gravity of soil particles. It is always accompanied by the phenomenon of the "boiling" or "heaving" of both coarse and fine particles. For cohesionless soils, i_c is approximately equal to 1.

The critical hydraulic gradient for internal erosion, i_s, corresponds to the minimum hydraulic gradient at which the first sign of internal erosion appears when the imposed hydraulic gradient gradually increases, indicated by the slight rushing out of fine particles. It corresponds to the inflection point in the hydraulic gradient and the flow velocity relationship curve.

3.2. Observed fine particle migration

All the test specimens, except Specimen D-30, showed internal erosion phenomena. The hydraulic behavior of

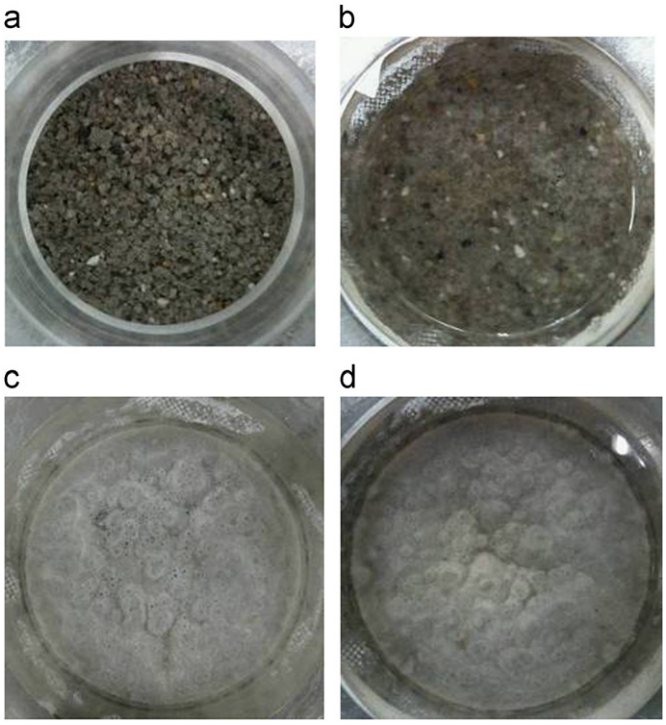

Fig. 6. Observed particle migrations from top (Specimen A-30). (a) Before internal erosion, (b) i=0.15, (c) i=0.20 and (d) i=0.23.

those specimens, such as the tendency of the flow velocity and the hydraulic gradient relation, is similar. Since the phenomenon observed in Specimen A is obvious and typical, the results of Specimen A are mainly shown later in the paper for discussion. Fig. 6 presents the observation of the fine particle loss from the top (Specimen A-30). Before the onset of the internal erosion, the fine particles stay still. When the critical hydraulic gradient for internal erosion is reached, small "dance-like" movements of fine particles occur. A very light layer of sand silt covers the top surface. Then, a few sand spots or sand volcanoes appear after increasing the hydraulic gradient. Slight movement of the fine particles is found around those spots. At the larger imposed hydraulic gradient, the number of sand spots increases and covers the whole area, and the movement of the fine particles around those spots becomes fiercer. As the hydraulic gradient is further increased, a piping-like phenomenon happens.

3.3. Onset of internal erosion

The typical relationship between the hydraulic gradient and the flow velocity (Specimen A-30) is shown in Fig. 7. At first, the approximate linear relationship between the hydraulic gradient and the flow velocity, in accordance with Darcy's law, indicates no occurrence of internal erosion. At this stage, the effective porosity, representing the porosity available for contribution to the fluid flowing through the specimens, stays basically the same irrespective of the hydraulic gradient. After reaching the critical hydraulic

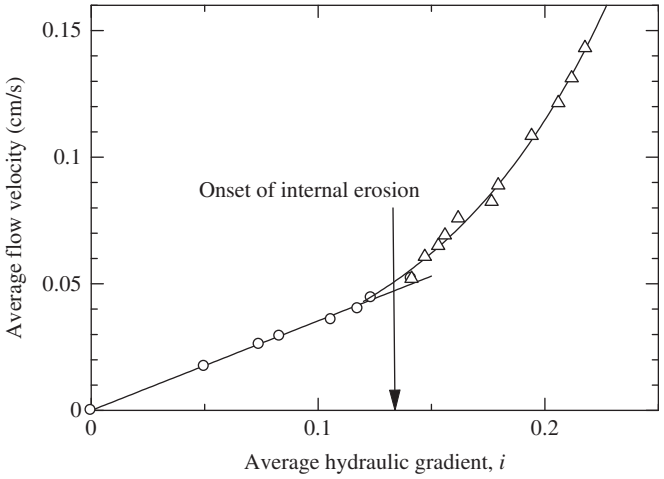

Fig. 7. Hydraulic gradient and flow velocity relation (Specimen A-30).

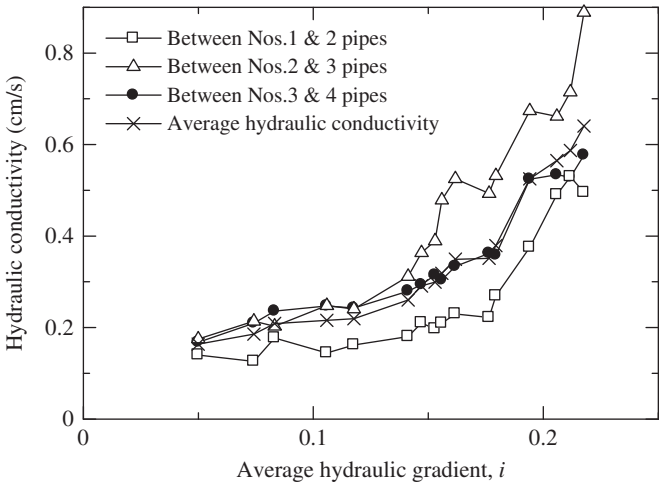

Fig. 8. Local hydraulic conductivity variance (Specimen A-30).

gradient for internal erosion i_s, the curve slope begins to inflect, corresponding to the first observation of "dance-like" movements of the fine particles. The fine particles are washed out by the seepage flow, leading to the increase in effective porosity, and thus, hydraulic conductivity. It can be inferred that when the critical hydraulic gradient for soil stability i_c is reached, the "heaving" phenomenon occurs and the specimen reaches the state of zero effective stress.

3.4. Hydraulic conductivity

Since the amount of fine particle loss varies with the depth, the hydraulic conductivity is not uniform for all depths. In this section, the changes in local hydraulic conductivity are calculated by the local hydraulic gradient assuming that the seepage flow follows Darcy's law. Fig. 8 shows the relationship between the average hydraulic gradient and the local hydraulic conductivity of each layer for Specimen A-30.

Before internal erosion ($i < 0.13$), a slight increase in the hydraulic conductivity with the imposed hydraulic gradient can be observed because of the nature of the upward seepage flow test, namely the upward flow would decrease the effective stress, similar to unloading the soil, and the void ratio would correspondingly increase, leading to the increase in hydraulic conductivity even without internal erosion. However, compared to the drastic increments in hydraulic conductivity, due to the loss of fine particles, the hydraulic conductivity is thought to be basically constant before internal erosion and its increments could be negligible. After the onset of internal erosion, the hydraulic conductivity obviously increases with the imposed hydraulic gradient, resulting in three times the initial value when the maximum imposed hydraulic gradient of 0.22 is reached. The loss of fine particles would lead to the increase in hydraulic conductivity.

3.5. Influence of controlled factors

Fig. 9 shows the variance in the critical hydraulic gradient for soil stability and the critical hydraulic gradient for internal erosion with the different initial fine contents for the dense soil specimen (60% relative density). The calculated critical hydraulic gradient for zero effective stress following, Terzaghi's equation, are 1.08, 1.06, 1.05 and 1.03, and the experimental values of the critical hydraulic gradient for internal erosion are 0.21, 0.23, 0.24 and 0.25, respectively. These values are in accordance with the test results of Skempton and Brogan (1994), namely migration and the strong piping of fines take place in unstable materials at gradients of about one-fifth to one-third of the theoretical value. There seems to be a trend for the specimen with a lower fine content to require a larger hydraulic gradient in order to initiate internal erosion. The loose specimens also show the same trend (Fig. 10).

The influence of the relative density on the critical hydraulic gradient for internal erosion is presented in Fig. 11. A larger relative density for the specimen with the same fine content leads to a larger value of critical hydraulic gradient for internal erosion.

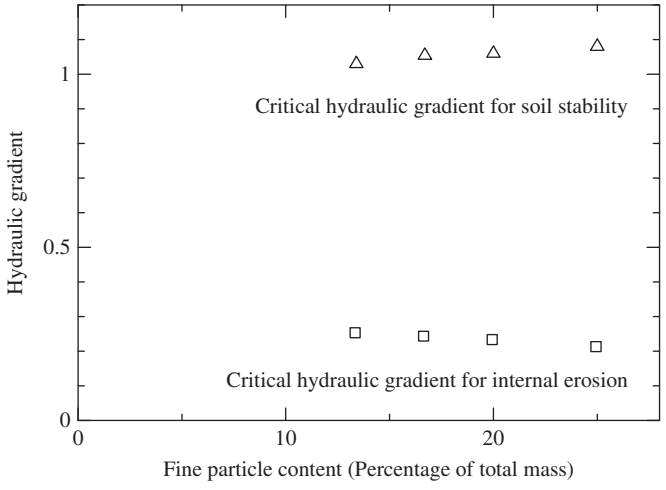

Fig. 9. Relation between fine content and i_s, i_c for dense samples.

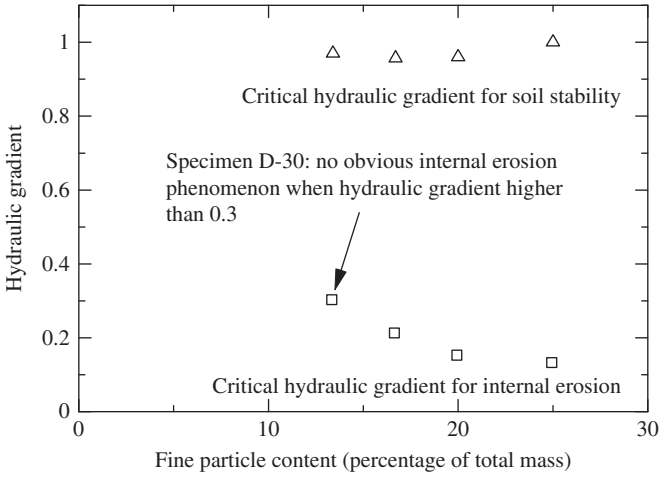

Fig. 10. Relation between fine content and i_s, i_c for loose samples.

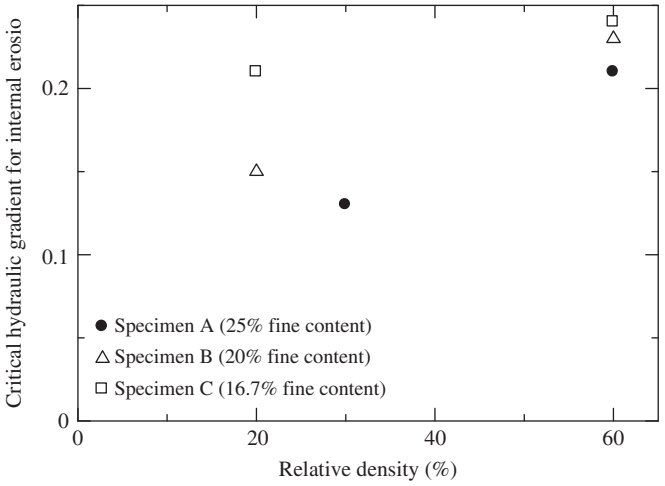

Fig. 11. Relationship between relative density and i_s.

3.6. Fine particle loss during internal erosion

Typical post-test particle size distribution curves for each zone (Fig. 5) of Specimen A-60 at $i_{max}=0.45$ are shown in Fig. 12. The distribution curve for each layer, after the internal erosion shifts downward from the original curve after internal erosion, indicates that there has been a fine particle loss. The extent of the movement proportionally increases with the amount of fine particle loss. A graphical method proposed by Kenney and Lau (1985) is used to approximately assess the fraction of eroded fine particles, as well as the largest eroded fine particles, based on the changes in the particle size distribution curve. A detailed calculation is shown in Fig. 13. The main idea of this method is to extend the initial particle size distribution curve of the test sample to match the curve after internal erosion. Since the coarse particles stay the same after internal erosion, by extending the

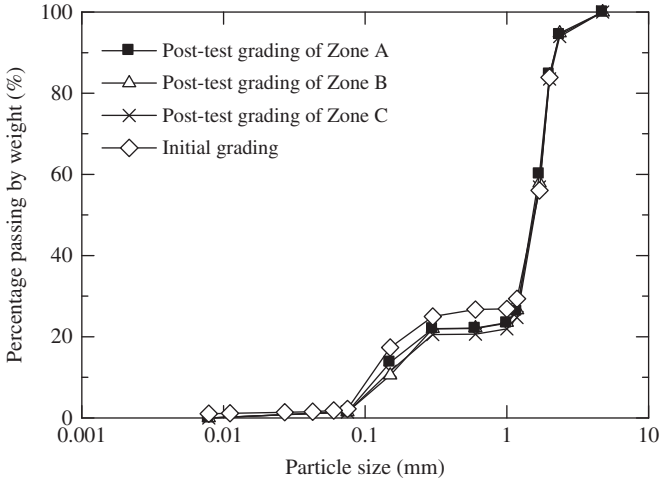

Fig. 12. Particle size distribution curve with depth.

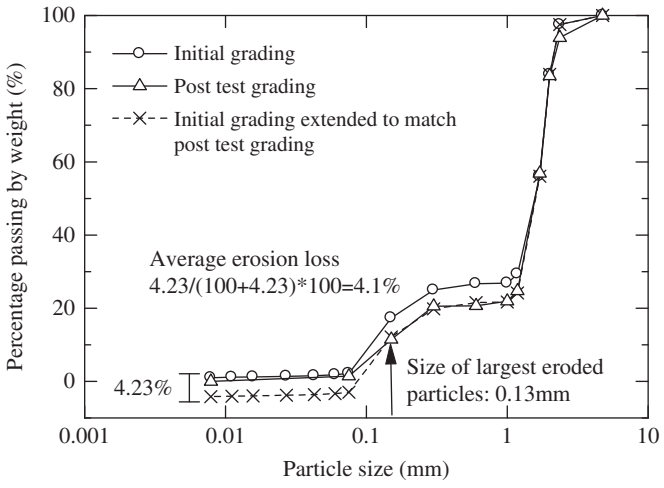

Fig. 13. Graphical method of fine particle loss assessment.

vertical scale of the initial particle size distribution curve, the coarse part of the initial curve should match that of the post-test particle size distribution curve. The fraction of eroded fine particles can be calculated from the amount of movement of the initial particle size distribution curve.

Table 6 presents the particle loss (percentage of total mass) after imposing two different maximum hydraulic gradients for Specimen A-60. It is noted that the fine particle loss of the bottom layer is the greatest, since the bottom layer has no "fine particle supply". The fine particles are washed away leading to a large amount of particle loss. For the middle and upper layers, although their fine particles are washed away by the seepage flow, the fine particles from the bottom layer are dragged up by the seepage flow, forming a particle supplement to those layers. Due to the open-ended nature of the water channel, more particles will be eroded from the top layer than from the middle layer. This finding is in accordance with Kenney and Lau (1985). They defined the three layers as the top transition zone, the central homogeneous zone and the

Table 6
Fine particle loss at different depths for SpecimenA-60.

Zones	Particle loss (%)	
	0.45[a]	0.51[a]
Zone A	3.00	3.00
Zone B	2.70	2.94
Zone C	4.10	5.11

[a]Maximum imposed hydraulic gradient.

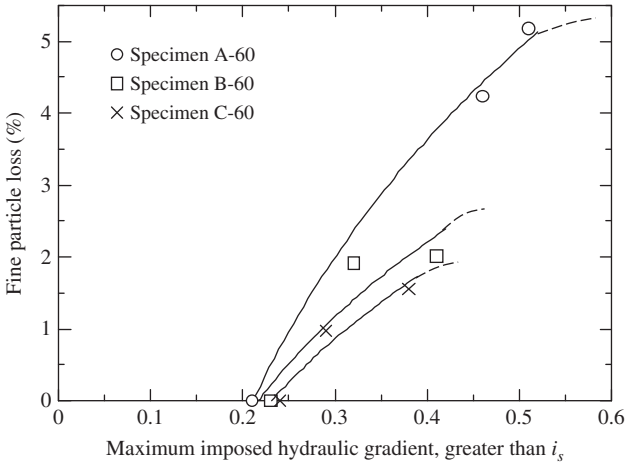

Fig. 14. Fine particle loss variance with maximum imposed hydraulic gradient at various fine contents.

bottom transition zone. The particle loss in the top and bottom zones is larger than that in the central zone.

For Specimens A-60, B-60 and C-60, different maximum hydraulic gradients, larger than the critical hydraulic gradient for internal erosion, are imposed to find its influence on the fine particle loss. The relationship between the maximum imposed hydraulic gradient and the fine particle loss of those specimens with different fine contents are shown in Fig. 14. There is a general trend that the larger maximum imposed hydraulic gradient means a larger fine particle loss. Specifically, before the onset of the internal erosion, the soil specimens are stable without any fine particle loss. Once internal erosion starts, the particle loss increases with the imposed hydraulic gradient. At the same imposed hydraulic gradient, the specimen with the larger fine content shows the potential for more erosion. Due to the relatively large hydraulic conductivity of the tested specimens, a hydraulic gradient of greater than 0.51 cannot be imposed. Since the amount of erodible fine particles in a mixture is definite, the eroded fine particles will not increase unlimitedly with the imposed hydraulic gradient. When a certain hydraulic gradient is reached, the fine particle loss will be close to its limit and remain stable irrespective of the hydraulic gradient.

3.7. Void ratio and volumetric deformation

An obvious characteristic of internal erosion is the change in soil microstructure, resulting in the increase in

void ratio and volumetric deformation. Due to the nature of the upward seepage tests, the precise measurement of the soil deformation during the seepage tests cannot be conducted. By observation, there is a trend that the tested specimens subsides after internal erosion (Fig. 15). The largest deformation is observed at Specimen A-60. The volumetric strain caused by internal erosion is about 6%. The specimen deformation is caused by both the loss in soil particles and the possible change in voids due to the soil particle spatial adjustment, as is shown in Fig. 16. The largest increase in void ratio occurs if there is no deformation during the internal erosion, corresponding to the Mitchell (1976) assumption that the fine particles occupy the voids between the coarse particles and may not participate in the force transfer. The loss of those fines would not cause any deformation in the soil fabric. The minimum volumetric strain is 0. However, in practice, the internal erosion would always be accompanied by the deformation of the soil structure, which is regarded as a sign of instability. It may be better to consider this possibility as an ideal simplification in theory. The minimum void ratio of the specimen after erosion could be estimated by the greatest compaction that the coarse particles could achieve, resulting from the rearrangement of the soil particles. Under this circumstance, the volumetric deformation of the specimen would reach the maximum value.

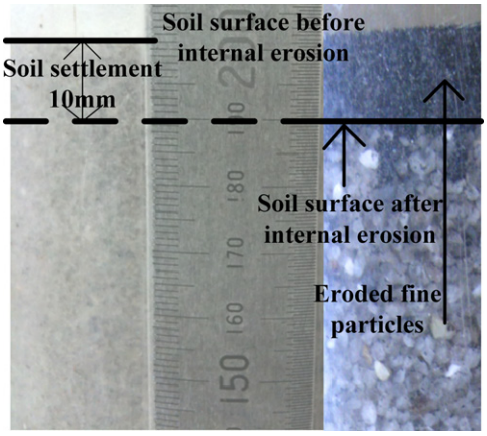

Fig. 15. Changes in soil volume due to internal erosion (Specimen A-60).

The soil volumetric deformation is accompanied by the possible loss of those fines actively engaged in the mechanical transfer and the spatial rearrangement of the soil particles, both of which would probably adjust the force transfer path in specimens, and consequently, lead to a reduction in soil strength after internal erosion.

4. Cone penetration test (CPT)

Due to the difficulties of retrieving undisturbed samples from the seepage cell after the tests, an in situ testing technique is needed to characterize the mechanical properties of the specimen. The miniature cone penetration test (CPT) was selected because it offers the continuous measurement of the cone resistance along depth and excellent repeatability. In practice, the friction angle of sand deposits can be estimated from the results of CPTs (Terzaghi et al., 1996). By conducting CPTs before and after the application of the seepage flow to the specimen, the reduction in strength due to the internal erosion can be evaluated. The miniature cone used in the tests is a cylindrical cone tip with a diameter of 10 mm and tip apex angles of 60° (Fig. 17). By using an embedded load cell, the resistance at the tip can be measured. A jack is connected to the upper end of the penetrometer to push the cone into the specimens at a constant rate. The data acquisition system allows automatic cone tip resistance recording. The penetration rate is 20 mm/s, following JGS 1435-2003. The total penetration depth is 160 mm. According to Been et al. (1986), who reviewed the problems associated with calibration chamber tests, the size effect, including particle size and the chamber size effect, and the boundary effect are the most important issues. The diameter ratio of seepage cell to cone in this research is 10, which might cause the size effect. Some assessments on the size effect in this study can be found in the Appendix. All the test specimens are listed in Table 7.

4.1. Cone resistance profile

Profiles of the cone tip resistance for Specimen A, B, C and D at 60% relative density are shown in Fig. 18. A larger fine content leads to a smaller cone tip resistance.

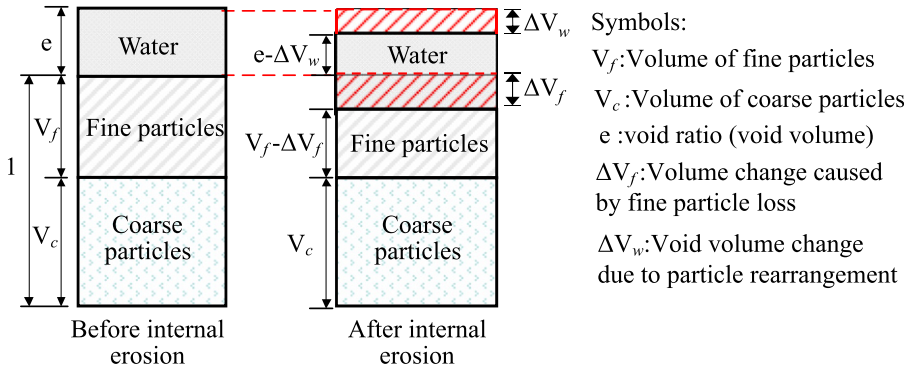

Fig. 16. Possible volumetric deformation of specimen.

Fig. 17. Miniature cone penetrometer.

Table 7
Number of specimens undertaken by CPT.

Specimen no.	Before internal erosion	After internal erosion
A-30	1 test	1 test
A-60	1 test	3 tests[a]
B-20	1 test	1 test
B-60	1 test	2 tests[a]
C-20	1 test	1 test
C-60	1 test	2 tests[a]
D-30	1 test	–
D-60	1 test	1 test

[a]For the dense specimens, seepage tests ending at different imposed hydraulic gradients were performed.

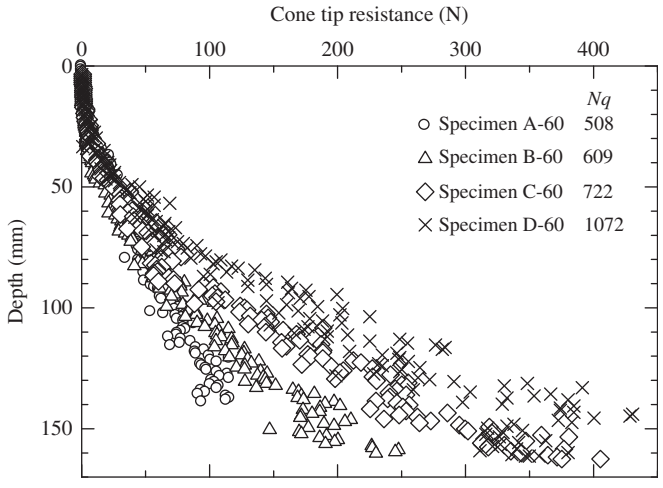

Fig. 18. Cone resistance of dense specimens.

A potential explanation is that for gap-graded soil, coarse particles work as the soil skeleton and the interlocking between them is primary. The fine particles work as separators between the coarse particles. With more fine content, those "separators" decrease the frictional forces between the coarse particles, resulting in a smaller shearing resistance and, correspondingly, a decrease in the cone tip resistance.

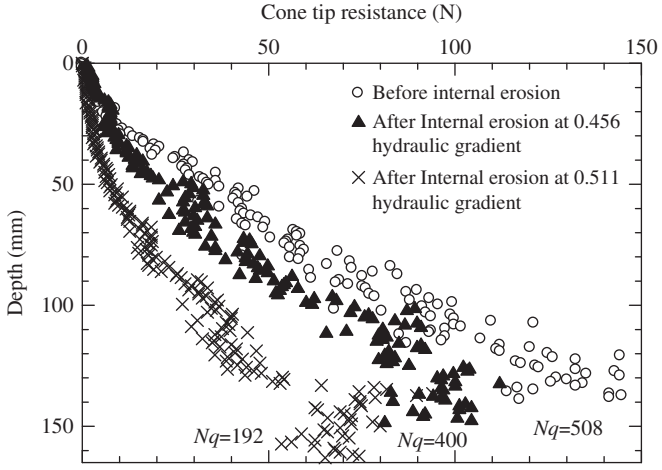

Fig. 19. Cone resistance before and after internal erosion (Specimen A-60).

The influence of internal erosion on CPTs is demonstrated by the cone tip resistance profiles obtained before and after the internal erosion. As an example, those of Specimen A-60 are shown in Fig. 19. After the internal erosion, the cone resistance decreases, indicating that the internal erosion process may have changed the interlocking of the soil particles leading to the decrease in cone resistance. However, the strength reduction may potentially be induced by fine particle loss, weakening soil particle interlocking or the size effect. In previous researches, the size effect was closely related to the relative density of soil. As the relative density is not very large (60% maximum), it can be said that the reduction in resistance is mainly caused by the fine particle loss, not by the size effect.

Fig. 19 also reveals that the reduction in cone tip resistance has a certain relationship with the maximum imposed hydraulic gradient. Before internal erosion, the soil structure is assumed to remain constant irrespective of the hydraulic gradient. After the onset of the internal erosion, the larger imposed maximum hydraulic gradient results in more fine particle loss, and therefore, further cone tip resistance reduction.

4.2. Cone resistance interpretation

The CPT data are interpreted into a mechanical parameter to make the CPT results easier to understand from an engineering point of view and to compare them with different cases. The approach of the interpretation is to develop empirical correlations between the cone tip resistance and the behavioral properties of soils (e.g., the angle of shearing resistance) based on various theories. Cone tip resistance is the measurement of the CPTs, and the

behavioral properties of the soils are obtained from laboratory tests. The most practical model explaining the cone tip resistance is the bearing capacity theory; it is based on the limit equilibrium method proposed by Terzaghi (1943). This method assumed the failure mechanisms and then determined the failure load by assuming that the soil was a rigid-plastic material. However, it was criticized for not taking the soil compressibility into account, leading to unreliable predictions of the angle of shearing resistance (Vesic 1972). However, Janbu and Senneset (1974) reported a relationship between bearing capacity number N_q, the ratio of cone resistance Δq_c and vertical effective stress $\Delta\sigma'_v$, and the angle of shearing resistance with little data scattering which indicated the limited influence of the soil compressibility. Work by Al-Awkati (1975) further proved that, for quartz sands, the shear strength had more influence on the cone resistance than the compressibility, and therefore, the bearing capacity theory could provide reasonable predictions. For silica sand, it is reasonable to empirically correlate the bearing capacity number (N_q) derived from CPTs and the drained angle of shearing resistance (φ'), which may commonly be represented as follows:

$$\tan\varphi' = A_1 + A_2 \ \ln(\Delta q_c/\Delta\sigma'_v) \tag{6}$$

where $\Delta\sigma'_v$ is the vertical effective stress increment at the depths where cone tip resistance increment Δq_c is measured ($N_q = \Delta q_c/\Delta\sigma'_v$). A_1 and A_2 are the regression coefficients. Durgunoglu and Mitchell (1975) initially proposed a design chart to determine the angle of shearing resistance based on the bearing capacity theory. The curve fitting yields $A_1=0.215$ and $A_2=0.131$. This method is found to be applicable to sands with low compressibility. Based on the calibration chamber test results on normally consolidated, moderately compressible, predominantly quartz sands, Robertson and Campanella (1983) showed a correlation in the form of a design chart, the regression coefficients of which are $A_1=0.194$ and $A_2=0.147$.

Following the common calibration procedure, the interpretation is performed to compare the measured cone penetration resistance, in terms of N_q, and the measured angle of shearing resistance from direct shear box tests. Since the tested specimens (A, B, C, D) mainly consist of Silica no. 3, the frictional forces of which are primary in shear strength, several fully saturated specimens consisting only of Silica no. 3 sand, are tested as well for calibration purposes. Those cases correspond to the extreme consequences of erosion, namely all the fines are eroded. Details are given in Table 8. The calibration chamber is the same as that used in the seepage tests.

To avoid the possible bottom boundary effects, the cone resistance data for depths of 30 mm–100 mm are selected to evaluate bearing capacity number N_q. The bearing capacity number obtained from the cone resistance profile (Fig. 18) of Specimen A, B, C and D at a relative density of 60% are shown in Table 8. In the same way as with the cone tip resistance, the bearing capacity number also decreases with the fine content. The bearing capacity number can be thought of as a mechanical parameter that can characterize the cone tip resistance. A reduction in the bearing capacity number due to internal erosion can be seen from Fig. 19. After internal erosion, the bearing capacity number decreases and the extent of the decrease in the bearing capacity number seems to be dependent on the imposed hydraulic gradient. This trend can be clearly noted from Fig. 20, which shows the relationship between the maximum imposed hydraulic gradient and the normalized bearing capacity number (the ratio of the bearing capacity number before and after internal erosion). For Specimen A-60, after internal erosion at a hydraulic gradient

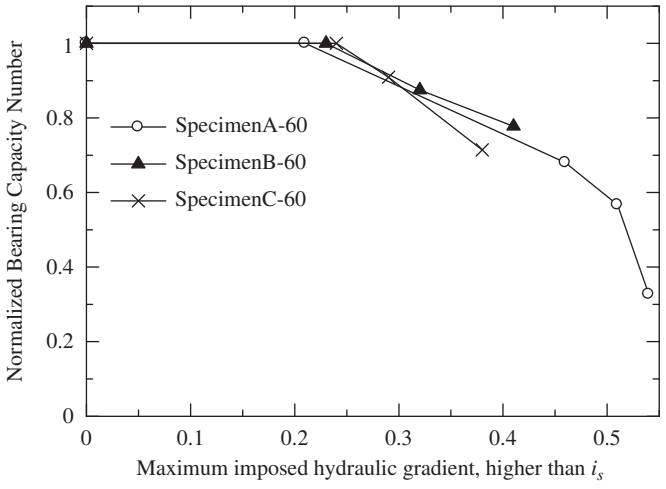

Fig. 20. Relation between maximum imposed hydraulic gradient and normalized bearing capacity number.

Table 8
Details of tested specimens in calibration studies.

Specimens	Relative density (%)	Void ratio	Mineralogy	Shape	Bearing capacity number
Silica no. 3	20	0.95	Mainly quartz	Subangular	26
Silica no. 3	60	0.82	Mainly quartz	Subangular	84
Silica no. 3	100	0.70	Mainly quartz	Subangular	938
Specimen A	60	0.51	Mainly quartz	Subangular	508
Specimen B	60	0.53	Mainly quartz	Subangular	609
Specimen C	60	0.54	Mainly quartz	Subangular	722
Specimen D	60	0.58	Mainly quartz	Subangular	1072

of 0.45, bearing capacity number N_q decreases by approximately 30%, while at a hydraulic gradient of 0.54, N_q decreases by about 70%.

The angles of shearing resistance of the tested specimens are obtained by conducting constant pressure direct shear box tests. The apparatus consists of shear boxes, a guide for the shear boxes and a loading system for both vertical force and shear force. The soil specimens are prepared by the moist tamping method, ensuring similar soil conditions as in the seepage tests. Each tested specimen is subjected to shearing at a velocity of 0.2 mm/min, following JGS 0560-0561, to allow volume changes of the specimen, while the effective normal stress on the shear plane is maintained at a constant value. For the same specimen, four different normal stresses, 25 kPa, 50 kPa, 100 kPa and 200 kPa, are conducted. Typical shearing results for Specimen A-60 are shown in Fig. 21.

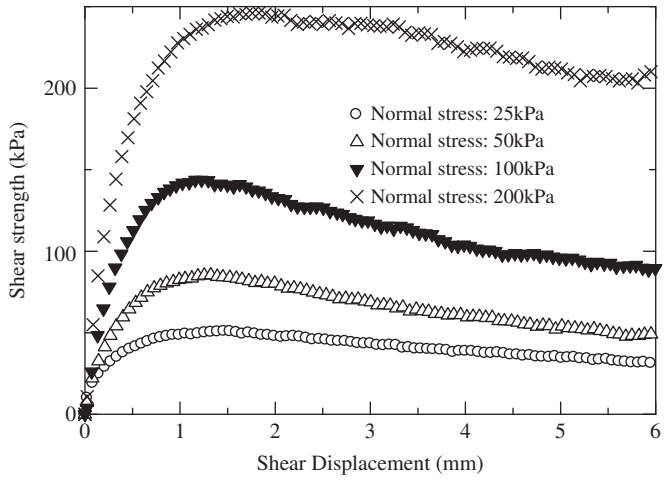

Fig. 21. Relation between shearing displacement and strength (Specimen A-60).

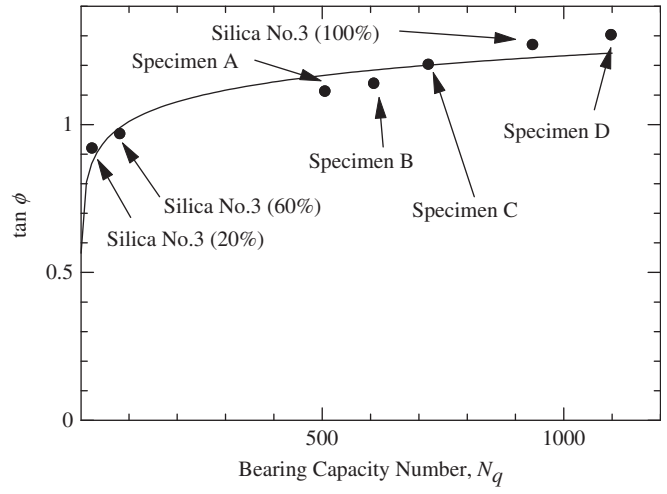

Fig. 22. Relation between bearing capacity number and tan ϕ.

The comparison between the bearing capacity number from the CPT data and the angle of shearing resistance obtained from the direct shear box tests is shown in Fig. 22. Due to the influence of compressibility, there is some scattering in the results. The best fitting curve by the logarithmic function is shown as follows:

$$\tan\varphi' \approx 0.573 + 0.1 \ln(\Delta q_c / \Delta \sigma_v') \quad (7)$$

Since this empirical correlation compares two different shear modes, i.e., simple shear in the direct shear box and compression at the cone tip, it underestimates the angle of shearing resistance value due to the influence of compressibility (Robertson and Campanella, 1983); and therefore, the strength reduction index in terms of $\tan\varphi'$ may not reflect the actual strength reduction quantitatively. However, at least it may shed some light on how the internal erosion affects the strength parameter in general.

To make the comparison clear, the strength reduction is defined as the following based on this correlation:

$$\Delta R = 1 - \frac{\tan\varphi'_{\text{post-erosion}}}{\tan\varphi'_{\text{before-erosion}}} \quad (8)$$

where ΔR is the strength reduction by percentage after erosion, $\varphi'_{\text{post-erosion}}$ is the angle of shearing resistance after internal erosion and $\varphi'_{\text{before-erosion}}$ is the angle of shearing resistance before internal erosion.

Changes in the soil strength due to internal erosion for both the loose and the dense specimens are summarized in Table 9. After internal erosion, the cone tip resistance decreases, resulting in a decrease in the estimated angle of

Table 9
Summary of changes in soil strength due to internal erosion.

Specimen no.	Normalized bearing capacity number	Angle of shearing resistance (deg.)		Strength reduction, ΔR (%)	Max. imposed hydraulic gradient
		Before internal erosion	After internal erosion		
A-30	0.86	36.1	35.8	1.0	0.22
B-20	0.96	32.7	32.6	0.3	0.25
C-20	0.95	35.1	35.0	0.3	0.24
A-60	0.33	41.1	39.5	6.1	0.54
B-60	0.78	41.6	41.2	1.4	0.41
C-60	0.71	42.1	41.6	1.8	0.38
D-60	0.67	42.4	41.8	2.1	0.28

shearing resistance. The fine particle loss varies depending on the imposed hydraulic gradients. The relationship between the maximum imposed hydraulic gradient and the normalized soil strength ($1-\Delta R$) is shown in Fig. 23. The larger imposed hydraulic gradient causes a further reduction in soil strength. Up to the imposed hydraulic gradient of 0.5, the changes in strength are gentle, while drastic changes can be seen with imposed hydraulic gradients over 0.5. However, the fine particle loss does not increase with the imposed hydraulic gradient unlimitedly. Due to the limitation of the system, the authors could not impose a large hydraulic gradient on the samples. It could be inferred, however, that at a certain stage, the particle loss may be constant irrespective of the imposed larger hydraulic gradient. Correspondingly, an upper limit for the reduction in soil strength, due to the internal erosion, may exist, as shown in Fig. 24. It is worth mentioning that the hydraulic gradient addressed here is within the range of i_s and i_c. Out of this range, the soil may be stable or may fail.

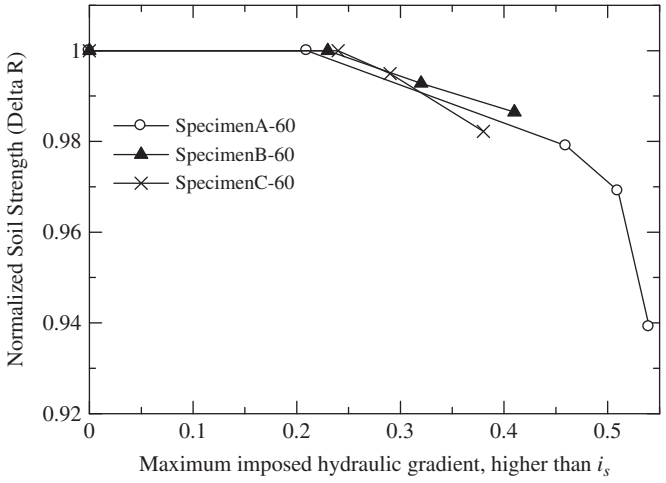

Fig. 23. Relation between maximum imposed hydraulic gradient and normalized soil strength.

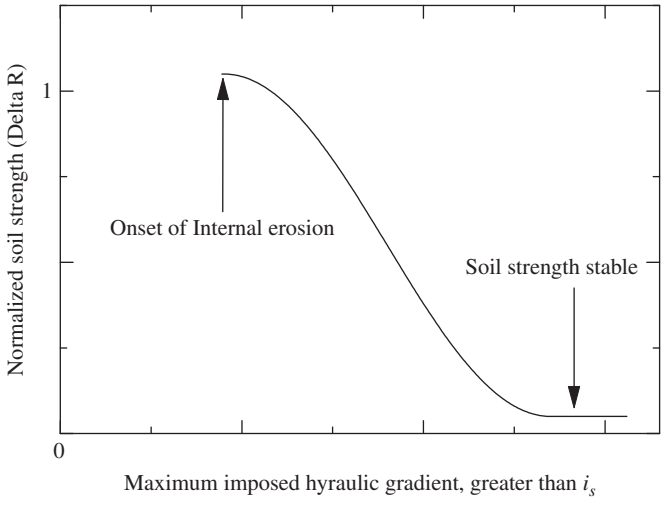

Fig. 24. Possible strength reduction curve against maximum imposed hydraulic gradient.

5. Conclusions

The influence of internal erosion on soil strength has been experimentally studied through a series of one-dimensional upward seepage tests at a constant water head and cone penetration tests. By giving an upward seepage flow to the gap-graded soil specimens, internally eroded soils were created. The mechanical consequences of internal erosion were examined by cone penetration tests on internally eroded specimens.

Before the internal erosion, the relationship between the average hydraulic gradient and the flow velocity is basically linear. After the onset of erosion, the slope of the relationship is no longer linear, indicating that the hydraulic conductivity of soils drastically increases with the progress of the internal erosion. The hydraulic gradient for internal erosion is found to be about one-fifth to one-third of the critical hydraulic gradient for soil stability. The lower the fine content, the larger the hydraulic gradient required to cause internal erosion. Those specimens containing the same mass ratio of fines as the larger relative density require a larger critical hydraulic gradient to initiate the internal erosion. The fine particle loss increases with the imposed hydraulic gradient.

The internal erosion causes a reduction in cone tip resistance, the extent of which may be related to the imposed hydraulic gradient. A larger imposed hydraulic gradient, indicating a greater loss of fine particles, would lead to further cone resistance reduction. Drastic changes in the strength can be seen with hydraulic gradients over 0.5. The internal erosion causes the angle of shearing resistance of a soil specimen to decrease within a certain hydraulic gradient range.

Appendix A. Size effects in CPT tests

A.1. Particle size effect

Due to the comparatively large particle size of Silica no. 3, the particle size effect, characterized by the ratio of cone diameter to mean particle size, should be considered. Gui and Bolton (1998) introduced the new concept of "effective diameter", which is the sum of the cone diameter and the mean particle size, to erase the particle size effect. The effective diameter was considered in the interpretation of the test data in this study. The mean particle size was obtained from the particle size distribution curve before and after the seepage test.

A.2. Chamber size effect

Chamber size and imposed boundary conditions are influential on cone resistance. Detailed discussions can be found in Been et al. (1986, 1987), Mayne (1991), and

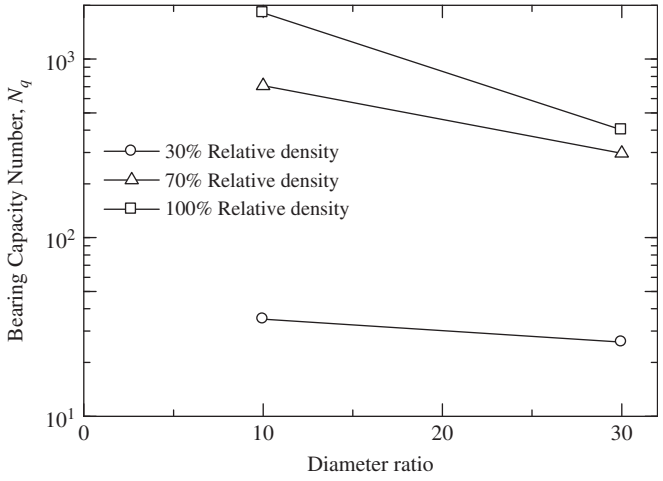

Fig. A1. Relation between bearing capacity number and diameter ratio.

Schnaid and Houlsby (1991), among others. Even though many studies have been conducted on this issue, it appears that there are no universally accepted explanations. Generally, the chamber size effect is less for loose sand, while for medium and dense sand, the size effect depends on the chamber-to-cone diameter ratio, stress state and so on.

To assess the size effect, CPT tests were conducted using a 300-m-diameter container with a diameter ratio of 30 as well as a seepage cell with a diameter ratio of 10. The dry Silica no. 3 specimen was prepared in the above-mentioned two containers by the air pluviation method. Three relative densities corresponding to loose (Dr=30%), medium (Dr=70%) and dense (Dr=100%) states are considered. In terms of bearing capacity number N_q, the effect of the container diameter is plotted in Fig. A1. As expected, the size effect becomes much more obvious with a larger relative density. Due to the comparatively small relative densities of the tested specimens in these tests, this effect was not considered in the interpretation of the test data in this study.

References

Al-Awkati, Z.A., 1975. On Problems of Soil Bearing Capacity at Depth. Ph.D. Thesis, Department of Civil Engineering, Duke University, Durham, NC.

U.S. Army Corps of Engineers, 1953. Filter Experiments and Design Criteria. Technical Memorandum. Waterways Experiment Station, Vicksburg.

Been, K., et al., 1986. The cone penetration test in sands. Part 1: state parameter interpretation. Geotechnique 36 (2), 239–249.

Been, K., et al., 1987. The cone penetration test in sands. Part 2: general inference of state. Geotechnique 37 (3), 285–299.

Bradshaw, A.S., Baxter, C.D., 2007. Sample preparation of silts for liquefaction testing. Geotechnical Testing Journal 30 (4), 324–332.

Burenkova, V.V., 1993. Assessment of Suffusion in Non-cohesive and Graded Soils. Filters in Geotechnical and Hydraulic Engineering. Brauns, Heibaum & Schuler, Balkema, Rotterdam 357–360.

Durgunoglu, H.T., Mitchell, J.K., 1975. Static penetration resistance of soils: I-ANALYSIS. In: Proceedings of the ASCE Specialty Conference on In-situ Measurement of Soil Parameters, Raleigh, vol. 1.

Frost, J.D., Park, J.Y., 2003. A critical assessment of the moist tamping technique. Geotechnical Testing Journal 26 (1), 57–69.

Gui, M.W., Bolton, M.D., 1998. Geometry and scale effects in CPT and pile design. Geotechnical site characterization. Robertson & Mayne, 1063–1068.

Istomina, V.S., 1957. Filtration stability of soils. Gostroizdat, Moscow, Leningrad.

Janbu, N., Senneset, K., 1974. Effective stress interpretation of in situ static penetration tests. In: Proceedings of the European Symposium on Penetration Testing, ESOPT I, Stockholm, Sweden, vol. 2.2, pp. 181–193.

Kenney, T.C., Lau, D., 1985. Internal stability of granular filters. Canadian Geotechnical Journal 22, 215–225.

Kenney, T.C., Lau, D., 1986. Internal stability of granular filters. Canadian Geotechnical Journal 23, 420–423.

Ladd, R.S., 1978. Preparing test specimens using undercompaction. Geotechnical Testing Journal 1 (1), 16–23.

Mao, C.X., 2005. Study on piping and filters: part 1 of piping. Rock and Soil Mechanics 26 (2), 209–215.

Mayne, P.W., 1991. Determination of OCR in Clays by Piezocone Tests using cavity expansion and critical state concepts. Soils and Foundations 31 (2), 65–76.

Mitchell, J.K., 1976. Fundamentals of Soil Behavior. Wiley, New York.

Moffat, R.A., Fannin, R.J., 2006. A large permeameter for study of internal stability in cohesionless soils. Geotechnical Testing Journal 29 (4), 273–279.

Omine, K., Ochiai, H., 1992. Stress–strain relationship of mixtures with two different materials and its application to one-dimensional compression property of sand-clay mixed soils. In: Proceedings of Japan Society of Civil Engineers, no. 448/III-19, pp. 121–130 (in Japanese).

Omine, K., Ochiai, H., Yasufuku, N., 1996. Evaluation of strength–deformation properties of light-weight soils based on two-phase mixture model. In: Proceedings of the Twelfth Southeast Asian Geotechnical Conference, Kuala Lumpur, pp. 101–106.

Robertson, P.K., Campanella, R.G., 1983. Interpretation of cone penetration test. Part I: sand. Canadian Geotechnical Journal 20, 718–733.

Schnaid, F., Houlsby, G.T., 1991. An assessment of chamber size effects in the calibration of in situ tests in sand. Geotechnique 41 (3), 437–445.

Skempton, A.W., Brogan, J.M., 1994. Experiments on piping in sandy gravels. Geotechnique 44 (3), 449–460.

Terzaghi, K., 1943. Theoretical Soil Mechanics. John Wiley and Sons, INC.

Terzaghi, K., Peck, R.B., 1948. Soil Mechanics in Engineering Practice, first ed. John Wiley and Sons, New York.

Terzaghi, K., Peck, R.B., Mesri, G., 1996. Soil Mechanics in Engineering Practice, third ed. John Wiley and Sons, INC.

Thevanayagam, S., Mohan, S., 2000. Intergranular state variables and stress–strain behavior of silty sands. Geotechnique 50 (1), 1–23.

Tomlinson, S.S., Vaid, Y.P., 2000. Seepage forces and confining pressure effects on piping erosion. Canadian Geotechnical Journal 37, 1–13.

Vallejo, L.E., 2001. Interpretation of the limits in shear strength in binary granular mixtures. Canadian Geotechnical Journal 38, 1097–1104.

Vesic, A.S., 1972. Expansion of cavities in infinite soil masses. ASCE Journal of the Soil Mechanics and Foundations Division 96 (SM3), 265–290.

Wan, C.F., 2006. Experimental Investigations of Piping Erosion and Suffusion of Soils in Embankment Dams and Their Foundations. Ph.D. Thesis. School of Civil and Environmental Engineering, University of New South Wales.

Yang, Z.X., Li, X.S., Yang, J., 2008. Quantifying and modeling fabric anisotropy of granular soils. Geotechnique 58 (4), 237–248.